

Z Dependence of the Laser-Intensity Threshold for Inhibited Electron Thermal Conduction

G. McClellan, P. H. Y. Lee, and G. Caporaso

University of California, Lawrence Livermore Laboratory, Livermore, California 94550

(Received 28 August 1979)

Temporally resolved sub-kiloelectronvolt x-ray emission pulses have been obtained from disk targets illuminated with 1.06- μm wavelength laser light at 5×10^{14} W/cm². Striking variations in the x-ray pulse shape from Be, Ti, Sn, Au, and U targets indicate the onset of strongly inhibited electron thermal conduction during the rise of the laser intensity. The laser intensity threshold for this strong inhibition is found to increase with target atomic number Z .

In this Letter we present a systematic dependence on target atomic number Z of the temporally resolved sub-kiloelectronvolt x-ray emission from disk targets illuminated with 1-ns, 1.06- μm wavelength laser pulses at a nominal intensity of 5×10^{14} W/cm². We interpret the temporal behavior of the sub-kiloelectronvolt x-ray emission as showing the onset of strongly inhibited electron thermal conduction during the rise of the laser intensity. As the Z of the target material is reduced, this strong conduction inhibition occurs earlier, i.e., at lower intensity.

There is substantial experimental evidence¹⁻¹⁰ that electron heat conduction in plasmas produced by 1.06- μm laser intensities above 10^{14} W/cm² is inhibited. The existence of an intensity threshold for this effect has been clearly demonstrated by Pearlman and Anthes³ with measurements of the front and rear plasma thermal expansion velocities from a thin polystyrene film. We extend the idea of an intensity threshold for inhibited conduction to include a Z dependence of the threshold.

Mechanisms that have been discussed which will inhibit electron thermal conduction of laser irradiated targets include self-generated magnetic fields,¹¹ ion acoustic turbulence,¹² and electrostatic fields set up by suprathermal electrons.¹³ Data on the dependence of inhibition on parameters such as laser intensity, pulse width, wavelength, spot size, target material, and beam uniformity should bring a better theoretical understanding of conduction inhibition and help determine the dominant mechanism(s). We report on the Z dependence.

The experiments were performed at 1.06- μm wavelength with one beam of the Argus laser facility,¹⁴ operating with nominal 800-J, 1-ns full width at half maximum (FWHM), Gaussian pulses. The nominal intensity on the target was 5×10^{14} W/cm² with a 450- μm diameter spot. The targets were disks, 600-700 μm in diameter and

13-25 μm thick. Target materials were Be, Ti, Sn, Au, and U. The instrument used for the time-resolved low-energy x-ray measurements is the Dante-T system,¹⁵ which is a ten-channel, filtered, x-ray diode detector system. The channel responses lie between 250 and 1500 eV. The FWHM of the channel response times range from 170 to 700 ps, depending on the oscilloscope used on each channel. The targets were irradiated by $f/2.2$ focusing optics, the incidence angle was 30° for all cases, and the Dante-T viewed the x-ray emission at an angle of 60° from the target surface normal in the plane of incidence, away from the incident beam. The beam was linearly polarized 14° out of the plane of incidence.

Figure 1 shows for a series of elements the pulse of 300-500-eV x-ray emission with a time resolution of 190 ps. Uranium shows a smooth, Gaussian-like pulse with a FWHM 1.5 times that of the incident laser pulse. As Z decreases, the pulses become flat-topped and the FWHM increases to nearly twice the laser pulse width at the lowest Z . Each element showed qualitatively similar pulse shapes for all channels of the Dante system.

We believe that the irregular pulse shapes for the lower- Z targets are caused by the onset of strong inhibition of electron thermal conduction as the incident laser intensity crosses a threshold level. The transition is shown most clearly by titanium. The x-ray emission starts to increase rapidly, presumably following the rise of the incident laser intensity. At a well-defined time, the x-ray emission abruptly switches to a slow linear rise and then drops after about 1 ns. This pattern reproduced on all three titanium shots. For tin, the change in slope occurs later (at a higher laser intensity) causing a lesser but definite effect on the x-ray pulse shape. For gold, the peak laser intensity apparently just gets to threshold since one shot showed a ripple at the top of the x-ray pulse and one showed a smooth

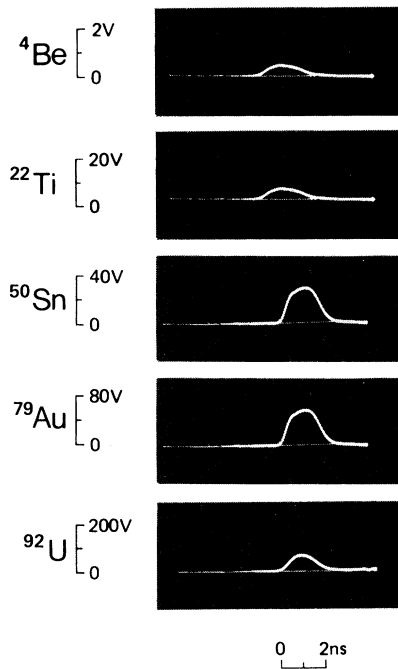


FIG. 1. Typical x-ray emission signals from disk targets illuminated with $1.06\text{-}\mu\text{m}$ laser light at $5 \times 10^{14} \text{ W/cm}^2$, 1 ns FWHM. A vanadium filter (L edge 520 eV) was used with an aluminum photocathode. Time resolution is 190 ps.

pulse. For uranium, three shots showed smooth x-ray pulse shapes, indicating that the laser intensity did not reach threshold for the transition.

This systematic variation of the x-ray pulse shape with Z indicates that the plasma process involved has a laser intensity threshold which increases with Z .

Data for gold disks were obtained both above and below threshold. Shots were taken with the same nominal incident energy (800 J in 950 ps) but with different spot size to produce peak intensities of 5×10^{14} and $3 \times 10^{15} \text{ W/cm}^2$. Figure 2 shows the x-ray pulses for the 600–900-eV channel with a time resolution of 170 ps. Initially the two pulses rise similarly, but the emission from the higher-intensity shot abruptly falls away as the threshold is crossed. All x-ray energy channels show this behavior. Only a small part of this reduction in x-ray emission at the higher intensity is due to reduced absorption¹⁶ of the incident laser light, since the time-integrated x-ray emission drops by 60% while the time-integrated absorption¹⁰ drops by only 25%.

From the data of Fig. 2, the laser intensity threshold for gold is estimated to be $(6^{+4}) \times 10^{14}$

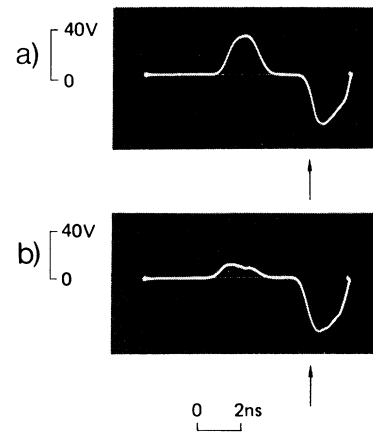


FIG. 2. X-ray emission signals from gold disks illuminated with 800 J for 1 ns with (a) $5 \times 10^{14} \text{ W/cm}^2$ and (b) $3 \times 10^{15} \text{ W/cm}^2$. The negative-going signal indicated by the arrow is a time fiducial. A copper filter (L edge 940 eV) was used with a chromium photocathode. Time resolution is 170 ps.

W/cm^2 . Even though the data of Fig. 1 lack time fiducials, it is clear that the threshold for uranium is greater than $5 \times 10^{14} \text{ W/cm}^2$ and that rough estimates of the thresholds for titanium and tin may be made. These results and the threshold for polystyrene from Ref. 3 are plotted in Fig. 3.

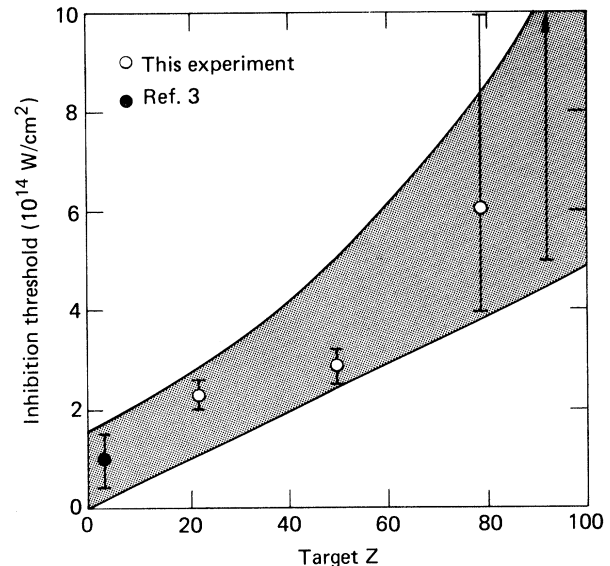


FIG. 3. The intensity threshold at $1.06\text{-}\mu\text{m}$ wavelength for strongly inhibited electron thermal conduction in laser-produced plasmas, vs the atomic number Z of the target material. The shaded area is meant to guide the eye.

Electron thermal conduction inhibition is a simple mechanism for regulating x-ray emission.¹⁰ The laser light is absorbed at and below the critical density surface which two-dimensional LASNEX¹⁷ numerical simulations indicate is 50 to 100 μm from the original target surface at the time of peak laser intensity. On the other hand, most of the sub-kiloelectronvolt x rays are emitted from the denser ablation layer within 20 μm of the original target surface. The absorbed laser energy must be transported by electron conduction from the underdense plasma to the overdense plasma. A decrease in electron thermal conductivity reduces the energy available for x-ray emission.

Calculated x-ray emission pulses from Ti are shown in Fig. 4 for three models of the plasma electron thermal conductivity. Curves *a* and *b* are typical of standard models in that they produce Gaussian-like pulses only 10% or 20% wider than the incident laser pulse. Curve *c* was produced by applying a time-varying multiplier to the Spitzer conductivity chosen to reproduce the 1.8-ns FWHM and flat-topped shape of the x-ray data. Above threshold, the conductivity multiplier required in the simulation varied inversely

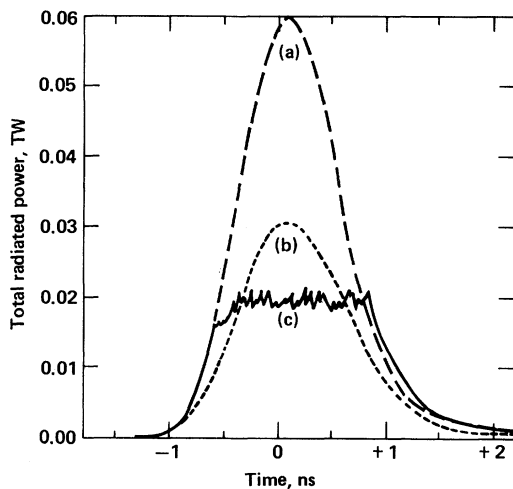


FIG. 4. X-ray emission vs time taken from numerical simulations of a Ti disk illuminated with 1.06- μm wavelength light (1 ns FWHM Gaussian pulse with peak intensity 5×10^{14} W/cm² at the time origin). The three curves correspond to models of the plasma electron thermal conductivity using flux-limited diffusion with (curve *a*) classical Spitzer conductivity, (curve *b*) flux limit reduced by ion acoustic turbulence, and (curve *c*) global conductivity multiplier varied in time to reproduce the experimentally observed x-ray emission.

with the $\frac{3}{2}$ power of absorbed intensity for both the rising and falling parts of the laser pulse, with a value of about 0.2 at 10^{14} W/cm² absorbed intensity. This result is not unique, since the laser light absorption versus time has not been measured. However, it does show that intensity-dependent conduction inhibition can produce the observed x-ray emission.

Since more than one inhibition mechanism may be operating, we do not rule out inhibition below the threshold of Fig. 3. In fact, the data presented here are consistent with previous results¹⁰ which showed the need for some inhibition in gold even at 3×10^{14} W/cm².

There are both theoretical and experimental reasons for believing that the variations in pulse shape are not a consequence of atomic structure differences of the targets. Our numerical simulations using ionization physics without the assumption of local thermodynamic equilibrium¹⁸ reproduce the qualitative features of the observed 0.2- to 1.5-keV x-ray spectra for all of the elements, but show no deviations from a smooth, Gaussian-like time dependence for the x-ray emission. Experimentally, the data for gold disks above and below the laser intensity threshold are decisive. In spite of a factor of 2.5 reduction in radiated energy for the higher intensity and a dramatic change in the x-ray emission pulse shape, only $\pm 15\%$ changes in the 0.2-1.5-keV spectral shape were observed. Thus, there is no correlation between atomic structure (as indicated by x-ray spectra) and the temporal behavior of the x-ray emission.

In conclusion, we have described the temporal behavior of the sub-kiloelectronvolt x-ray emission from 1.06- μm wavelength laser-illuminated disk targets at fixed spot size and intensity of 5×10^{14} W/cm². Abrupt temporal variations in the radiated power as the laser intensity rises have been interpreted as showing the onset of strongly inhibited electron thermal conduction in the laser-produced plasma. The laser intensity threshold for this effect is shown to increase with the *Z* of the target. Consequently, for a fixed laser intensity of a few times 10^{14} W/cm², electron thermal conduction is more strongly inhibited for low-*Z* targets than for high-*Z* targets.

The authors wish to thank G. B. Zimmerman, M. D. Rosen, and J. T. Larsen for illuminating discussions on the simulation of laser-plasma interactions. Theoretical background and experimental support has been provided by E. M. Campbell, K. G. Estabrook, W. L. Kruer, D. L. Mat-

thews, C. E. Max, K. G. Tirsell, and other colleagues in the Livermore Laser Fusion program.

This work was performed under the auspices of the U. S. Department of Energy, Contract No. W-7405-ENG-48.

¹R. C. Malone, R. L. McCrory, and R. L. Morse, *Phys. Rev. Lett.* **34**, 721 (1975).

²B. H. Ripin *et al.*, *Phys. Rev. Lett.* **34**, 1313 (1975).

³J. S. Pearlman and J. P. Anthes, *Appl. Phys. Lett.* **27**, 581 (1975).

⁴B. Yaakobi and A. Nee, *Phys. Rev. Lett.* **36**, 1077 (1976).

⁵W. C. Mead *et al.*, *Phys. Rev. Lett.* **37**, 489 (1976).

⁶F. C. Young *et al.*, *Appl. Phys. Lett.* **30**, 45 (1977).

⁷B. Yaakobi and T. C. Bristow, *Phys. Rev. Lett.* **38**, 350 (1977).

⁸P. M. Campbell, R. R. Johnson, F. J. Mayer, L. V. Powers, and D. C. Slater, *Phys. Rev. Lett.* **39**, 274 (1977).

⁹R. Benattar, C. Popovics, R. Sigel, and J. Virmont, *Phys. Rev. Lett.* **42**, 766 (1979).

¹⁰M. D. Rosen *et al.*, *Phys. Fluids* **22**, 2020 (1979).

¹¹J. A. Stamper *et al.*, *Phys. Rev. Lett.* **26**, 1012 (1971); for an extensive review see J. A. Stamper, U. S. Naval Research Laboratory Report No. 3872, 1978 (unpublished).

¹²D. W. Forslund, *J. Geophys. Res.* **75**, 17 (1970); R. Bickerton, *Nucl. Fusion* **13**, 457 (1973).

¹³E. J. Valeo and I. R. Bernstein, *Phys. Fluids* **19**, 1348 (1976).

¹⁴W. W. Simmons *et al.*, *Appl. Optics* **17**, 999 (1978).

¹⁵K. G. Tirsell, H. N. Kornblum, and V. W. Slivinsky, *Bull. Am. Phys. Soc.* **23**, 807 (1978).

¹⁶A change in the absorption mechanism has not been ruled out. Anomalous absorption in the far underdense plasma would shift the energy flow away from the overdense plasma toward more energetic plasma blowoff. For example, a buildup of ion-acoustic turbulence with increased laser intensity might simultaneously increase inhibition and cause anomalous absorption. R. J. Faehl and W. L. Kruer, *Phys. Fluids* **20**, 55 (1977); W. M. Manheimer, D. G. Colombant, and B. H. Ripin, *Phys. Rev. Lett.* **38**, 1135 (1977).

¹⁷G. B. Zimmerman, Lawrence Livermore Laboratory Report No. UCRL-74811, 1973 (unpublished).

¹⁸For a discussion of the physics modeling in these simulations, see Ref. 10.

Surface Diffusion by an Atomic Exchange Mechanism

John D. Wrigley and Gert Ehrlich

*Coordinated Science Laboratory, Department of Physics and Department of Metallurgy,
University of Illinois at Urbana-Champaign, Urbana, Illinois 61801*

(Received 31 December 1979)

On Ir(110), tungsten adatoms move preferentially across $[1\bar{1}0]$ channels rather than along them, as observed on other channeled planes. The jump mechanism underlying this anomalous behavior has been tested in an atom probe. It is found that after cross-channel motion, an iridium adatom is left on the iridium surface rather than the tungsten originally deposited. These observations provide the first experimental evidence for atomic diffusion on a metal by exchange of the adatom with an atom from the substrate.

In the past, it has generally been assumed that atomic diffusion on metals occurs by hopping over the surface. Observations of single metal atoms on channeled planes such as (211) of tungsten and (110) of rhodium¹ fit in well with this view. Migration on these surfaces is one dimensional (1D); as expected from the atomic arrangement of such planes, atoms move only in the direction of the surface channels. Recently, however, quite a different behavior has been found on some face-centered-cubic metals. On Pt(110), modeled in Fig. 1, Bassett and Webber² observed 2D diffusion of platinum and iridium atoms, with frequent movements across as well as along the $[1\bar{1}0]$ rows. On iridium (110), diffusion of iridi-

um and tungsten atoms occurs preferentially across the channels.³ Cross-channel motion of atoms may be visualized^{2,4} in two different ways: (1) via atomic jumps *over* the rows of lattice atoms forming the ridges, which *a priori* appear more unlikely than jumps along the channels; or (2) by an exchange process. In the latter, the adatom takes the place of a lattice atom in the side of the channel; it is the displaced lattice atom that continues the diffusion. We report here the first experimental evidence that cross-channel diffusion does, in fact, occur by an exchange mechanism.

The idea underlying our experiments is simple. Consider what happens when a foreign adatom,

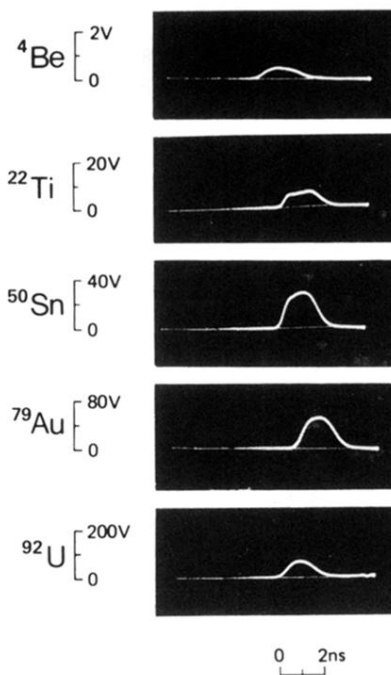


FIG. 1. Typical x-ray emission signals from disk targets illuminated with $1.06\text{-}\mu\text{m}$ laser light at $5 \times 10^{14} \text{ W/cm}^2$, 1 ns FWHM. A vanadium filter (L edge 520 eV) was used with an aluminum photocathode. Time resolution is 190 ps.

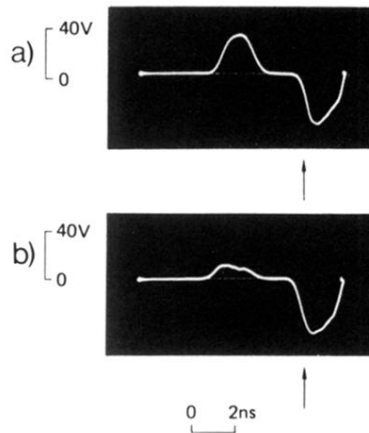


FIG. 2. X-ray emission signals from gold disks illuminated with 800 J for 1 ns with (a) 5×10^{14} W/cm² and (b) 3×10^{15} W/cm². The negative-going signal indicated by the arrow is a time fiducial. A copper filter (*L* edge 940 eV) was used with a chromium photocathode. Time resolution is 170 ps.